Journal of Hazardous Materials 504 (2026) 141297

Contents lists available at ScienceDirect

Journal of Hazardous Materials

journal homepage: www.elsevier.com/locate/jhazmat

Promoted photodegradation of cadmium pigment-embedded microplastics: Role of reactive microenvironment

Huiting Liu [a,b,*], Shijia Xu [a], Kexin He [b], Harald Oberhofer [c], Yuxuan Yao [c,d,**], Xiaolei Qu [b]

[a] School of Environmental and Chemical Engineering, Shenyang Ligong University, Liaoning 110159, China
[b] State Key Laboratory of Water Pollution Control and Green Resource Recycling, School of the Environment, Nanjing University, Jiangsu 210023, China
[c] Department of Physics and Bavarian Center for Battery Technologies, University of Bayreuth, Bayreuth 95447, Germany
[d] Department of Chemistry, TUM School of Natural Sciences, Technical University Munich, Garching 85748, Germany

HIGHLIGHTS

- Cadmium pigments promote photodegradation of PS, PP, and PE microplastics.
- Light-excited pigments create an active microenvironment, the key to this process.
- Polystyrene shows the strongest degradation due to proton attack on phenyl groups.
- DFT shows protonation allows carbocation and radical-driven degradation paths.
- The faster degradation of microplastics increases hazardous additive release.

GRAPHICAL ABSTRACT

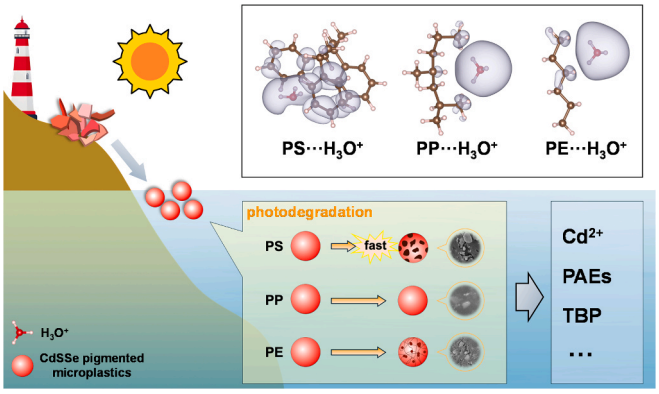

ARTICLE INFO

Keywords:
Microplastics
Photodegradation
Cadmium pigment
Acid catalysis
Plastic additives

ABSTRACT

The environmental fate of microplastics, largely derived from plastic fragmentation, is strongly influenced by their photodegradation behavior. While polymer degradation has been widely studied, less attention has been paid to the role of additives, particularly pigments used in colored plastics, in modulating these processes. This study investigates microplastics colored with cadmium pigments in three representative host polymers—polystyrene (PS), polypropylene (PP), and polyethylene (PE). The reactive microenvironment generated by the pigment includes electrons, holes, and protons through photo-induced reactions. Under this environment, PS was the most affected and exhibited accelerated degradation, attributed to proton attack at benzylic positions facilitated by its conjugated aromatic structure. Furthermore, we propose an additional pathway, where the photo-induced electron reduces the proton-induced carbocation to a radical, which will subsequently undergo oxidation reactions. Photodegradation, promoted by the pigment, correlates with its photodissociation and the concurrent release of Cd^{2+}. This effect is due to surface morphological changes that increase pigment exposure to irradiation. These findings demonstrate that pigment–polymer interactions significantly reshape degradation pathways. Notably, the accelerated degradation could increase the release of hazardous additives into water

* Corresponding author at: School of Environmental and Chemical Engineering, Shenyang Ligong University, Liaoning 110159, China.
** Corresponding author at: Department of Physics and Bavarian Center for Battery Technologies, University of Bayreuth, Bayreuth 95447, Germany.
E-mail addresses: huitingliu@sylu.edu.cn (H. Liu), yuxuan.yao@uni-bayreuth.de (Y. Yao).

https://doi.org/10.1016/j.jhazmat.2026.141297
Received 12 September 2025; Received in revised form 15 January 2026; Accepted 28 January 2026
Available online 2 February 2026

bodies, thus amplifying the environmental risks and revealing deficiencies in existing risk management strategies associated with microplastics.

1. Introduction

Over the past decades, plastics have revolutionized modern society due to their exceptional durability, affordability, and ease of manufacturing [24]. However, the widespread use of plastic products has led to a dramatic increase in plastic waste accumulation in the environment. It is reported that approximately 0.13–3.8 million metric tons of plastic waste enter the oceans from land-based sources each year, posing significant threats to freshwater, coastal, and marine ecosystems [69]. In the environment, plastic waste is subjected to long-term weathering, leading to the formation of increasingly smaller particles, with those less than 5 mm in size being referred to as microplastics [27, 57]. Microplastics have become ubiquitous in aquatic environments, and they are detected in lakes, rivers, oceans, and even the Arctic ice layer, especially in areas of high human activity [26,51]. Compared to large pieces of plastic, microplastics have a smaller diameter, a larger specific surface area, and their surface properties gradually change during the weathering processes (photodegradation, biodegradation, mechanical abrasion, and thermal oxidation, etc.) [70]. These factors imply that microplastics have a stronger capacity to carry environmental pollutants, and the endogenous additives are more likely to leach out, posing a greater environmental risk [35].

To achieve good appearance and functionality, plastic products are often colored by pigment additives. These pigments not only improve the visual attractiveness of plastic materials but also serve specific roles such as UV protection and thermal regulation. They are typically embedded within the polymer matrix and remain stable over time. As plastic waste fragments into microplastics through natural weathering, a diverse array of colorful microplastic particles is formed in the environment. Under prolonged exposure to sunlight and oxygen in marine environments, colored microplastics often undergo surface oxidation and discoloration, resulting in a prevalence of yellow and brown particles [42]. However, microplastics detected in fish bodies often exhibit a wider range of colors, including red, yellow, green, and blue, suggesting potential selectivity in ingestion or differences in exposure pathways [49,61]. The coloration of microplastics influences their environmental behavior. The pigments embedded in colored nano- and microplastics can act as light-shielding agents by absorbing certain wavelengths and energies of light. In addition, they may also participate in photochemical reactions, thereby affecting the photoaging and photodegradation processes of the plastic polymers [25,55,70]. The specific impact of pigments on photodegradation is influenced by multiple factors, including the type of polymer and the scale of plastic particles. For instance, it has been reported that the iron red pigment can significantly inhibit the surface photo-oxidation of polypropylene microplastics, while in polyethylene nanoplastics, the same pigment remarkably accelerates photoaging [36,48]. Meanwhile, the pigment additives in microplastics are likely to influence their ecological effects [64,9]. To be specific, some chemically toxic pigment additives are merely physically embedded within the polymer matrix, rather than chemically bonded. As a result, they are particularly prone to leaching during plastic weathering and degradation, posing potential environmental and ecological risks [23, 40,48,52]. These findings emphasize that pigments not only influence the physical leaching of toxic additives, but also actively alter the photodegradation behavior of microplastics. Despite this, systematic studies investigating how color and pigment composition affect the photodegradation of polymer particles remain limited.

Inorganic metal pigments are common additives in the polymer industry and are often found in plastic consumer goods like office supplies and daily necessities [60]. Among them, cadmium pigments—particularly cadmium sulfoselenide compounds—represent a prominent class of red inorganic metal pigments. Owing to their bright hues and thermal stability, these pigments perform particularly well in coloring polymers during high-temperature processing [12]. However, these advantages come with environmental trade-offs. The photochemical properties of cadmium pigments significantly enhance the environmental hazards of waste plastics containing these pigments when they enter natural water bodies. Our previous study demonstrated that photogenerated holes produced by light-excited cadmium pigments can oxidize the pigment lattice, inducing photodissolution and subsequent cadmium ion leaching [33]. When cadmium-pigmented polypropylene microplastics enter aquatic environments, the embedded pigment particles gradually dissolve through photoaging of the polymer matrix, resulting in sustained release of toxic cadmium ions. This release shows size dependency, increasing with decreasing particle size [34]. More concerning, cadmium-pigmented microplastics show strong toxicity to microalgae through two main mechanisms: light-blocking effects and the leaching of cadmium ions from the pigment. Together, these effects can impair primary production and potentially lead to broader ecological imbalances in aquatic systems. Wei et al., [65]. Recent studies suggest that the photochemical processes of cadmium pigments and plastic polymers may be closely coupled. On the one hand, cadmium pigments can significantly influence the photochemical behavior of the polymer matrix. For example, they have been shown to enhance the photoreactivity of polystyrene microplastics, effectively imparting photocatalyst-like properties to the particles [43]. In a recent study, Guo et al. synthesized $Cd_xZn_{1-x}Se_yS_{1-y}$ quantum dots based on the CdSSe structure and induced the degradation of PET plastics under visible light [17]. On the other hand, the photodegradation of microplastics can also affect the dissolution behavior of the pigments. Photoaged polystyrene microplastics have been reported to accelerate the photo-oxidative dissolution of cadmium pigments, which may paradoxically lead to a reduction in their acute aquatic toxicity, possibly due to transformation into less bioavailable forms [56]. Existing studies have largely focused on interactions between specific polymers and cadmium-based pigments. However, systematic assessments of polymer sensitivity in relation to structural and physicochemical properties are still lacking, leaving the underlying coupling mechanisms unclear. Pigment-polymer interactions directly influence the persistence, transformation, and ecological impact of colored microplastics in aquatic environments. A deeper understanding will not only improve environmental fate modeling but also support more accurate ecological risk assessments of pigmented microplastics in real-world conditions.

In this study, a commercial cadmium pigment (i.e., cadmium sulfoselenide pigment, CdSSe) was selected to synthesize colored microplastics (CdSSe-MPs) using three common types of hydrocarbon-based microplastics (polystyrene, polypropylene, polyethylene) found in aquatic environments. The photodegradation behavior of colored microplastics with the cadmium pigment was systematically studied. Under sunlight irradiation, the leaching kinetics of organics from colored microplastics were examined, and this was combined with qualitative and quantitative characterization of surface morphology and molecular structure to explore the specific effects of cadmium pigment on photodegradation. Mass spectrometry was employed to identify the plastic additives or additive intermediates leached from photodegraded MPs. Density functional theory (DFT) calculations were utilized to investigate the frontier orbitals of selected microplastic polymers. Understanding how polymer structural features govern both cadmium pigment photodissolution and microplastic photodegradation lies at the core of this work. Here, we directly connect polymer-dependent electronic structures with pigment–polymer photochemical coupling, revealing how different polymers modulate cadmium pigment

dissolution and microplastic transformation under irradiation. Our results show pronounced polymer-specific differences in sensitivity to cadmium pigments and uncover the regulatory mechanisms underlying these effects. Collectively, these findings extend the mechanistic understanding of pigmented microplastics beyond single-polymer systems and provide a scientific basis for both environmental risk assessment and the design of safer plastic materials and additives.

2. Materials and methods

2.1. Materials

Commercial cadmium pigment powder (cadmium sulfoselenide pigment, CdS_xSe_{1-x}) was purchased from Kela Co., Ltd., Xiangtan, China. The morphology and structural characterization data of cadmium pigment can be found in our previous researches [33,34]. Three types of polymer powders, including polystyrene (PS), polypropylene (PP) and polyethylene (PE), were purchased from Tesulang Co., Ltd., Dongguan, China. The polyethylene is of the high-density type. The polymer powders supplied by the supplier had a purity of approximately 95 %, and the compositions of the detected additives are detailed in Table S1. Lab-grade purified water (18.2 MΩ•cm) was produced by an ultra-pure water purification system (UPT-1–10T, ULUPURE, China).

2.2. Preparation of colored microplastics

The colored plastics pellets with varying polymer matrix compositions and pigment contents were synthesized using the plastics injection moulding machine (BP-QD-20S, Yilang Electromechanical Equipment Co., Ltd., Shanghai, China) with a 1 × 1 × 1 cm cubic mold. The specific injection molding process is described in detail in the Supplementary Material (cf. Text S1, Fig. S1 and Table S2). No additional additives were incorporated during the synthesis process. The plastics pellets were then mechanically pulverized into microplastic particles by a high-speed pulverizer (SS-1022, Haina Dianqi Co., Ltd., Jinhua, China). To prevent excessive temperature in the pulverizing chamber, each pulverization session was limited to no more than 5-min, coupled with physical cooling measures during the operation. The photochemical processes of colored microplastics containing cadmium pigment in aqueous phase are highly dependent on their particle sizes [34]. Therefore, microplastics with a particle size less than 0.15 mm were selected by sieving method for the characterization. The sieving of microplastics was conducted using a nylon mesh with a diameter of 10 cm and 100 mesh apertures, collecting the particles beneath the sieve, yielding CdSSe-MPs with particle sizes of less than 0.15 mm. The average particle size and corresponding distribution of the CdSSe-MPs are presented in Fig. S6.

Different mass fractions of cadmium pigments (0–30 wt%) were incorporated into three types of polymer matrices (PE, PP and PS) respectively. Cadmium pigments are typically incorporated into plastic consumer products at relatively low levels (0.1 %–1.2 %) owing to their strong tinting strength. The precise dosage is determined by the polymer matrix, product application, and desired color depth, and in most cases the content does not exceed 1 % [46]. In industrial practice, however, pigments are first blended with polymers to produce color masterbatches in order to ensure color uniformity and stability; these masterbatches typically contain substantially higher cadmium pigment contents, ranging from 10 % to 55 % [46]. The synthesis and preparation of the colored microplastics were subsequently carried out, and the resulting microplastic particles were individually sealed and stored in a light-free environment. The Fourier-transform infrared spectroscopy with attenuated total reflectance (ATR-FTIR, Nicolet iS20, Thermo, USA) method was utilized to characterize both the raw polymer materials and the resultant colored microplastics.

2.3. Irradiation experiments

The sunlight irradiation experiment involving CdSSe-MPs was conducted in deionized water, employing a 50 W Xe lamp (CEL-HXF300-T3, AULTT, China) as the simulate sunlight source. The experimental setup is depicted in Fig. S2. Prior to the commencement of the experiment, 250 mL of deionized water was injected into a 300 mL polytetrafluoroethylene (PTFE) beaker, and 70 mg of CdSSe-MPs powders was uniformly spread on the surface of the liquid. To ensure uniform light exposure during the experiment, the microplastic particles were arranged in a single layer without overlapping. The Xe lamp was placed at the top of the PTFE beaker, directing the light vertically onto the liquid surface. The light irradiation intensity was regularly monitored during the experiment using a light power meter (CEL-NP2000–2(10)A, AULTT, China) and was adjusted by controlling the height and output energy of the light source, keeping the light intensity steady at 95.17 ± 2.87 mW/cm^2. The spectrum of the Xe lamp, measured using a USB2000 + spectrometer (Ocean Optics, FL, USA), exhibits good agreement with that of natural sunlight (Fig. S2b). Simultaneously, the PTFE beaker was placed in a water circulating temperature control system (SDC-6, Scientz Biotechnology Co., Ltd., China), maintaining the reaction temperature at a constant 20 ± 0.1 °C. The initial pH of the reaction mixture was 6.75 ± 0.18 and was not adjusted. During irradiation, no appreciable pH fluctuations were observed, with the reaction system remaining within the neutral range (6.84 ± 0.42). Detailed pH variations for all irradiation experiments are provided in Fig. S3. During the irradiation, a disposable syringe was used to periodically sample the solution beneath the layer of CdSSe-MPs at set time intervals. To eliminate errors caused by liquid evaporation due to long-term irradiation, the evaporated water was replenished before each sampling. The sample collected was filtered using a 0.45 μm filter membrane (ANPEL Instrument Co., Ltd., Shanghai, China) to remove any possible microplastics.

2.4. Characterization of CdSSe-MPs and leaching products

The surface morphology and particle size distribution of CdSSe-MPs were analyzed using a scanning electron microscope (SEM, Merlin Compact, ZEISS, Germany). The functional groups of the microplastics were identified by ATR-FTIR spectroscopy over the wavenumber range of 400–4000 cm^{-1}. The surface elemental composition of the microplastics was characterized by X-ray photoelectron spectroscopy (XPS, Scientific K-Alpha, Thermo, USA) using a monochromatic Al Kα X-ray source. The dissolved small-molecule organic carbon concentration released from CdSSe-MPs during photochemical reactions was quantified using a total organic carbon analyzer (vario TOC, Elementar, Germany). The crystallinity of MPs was characterized using X-ray diffraction (XRD, D8 Advance, Bruker, Germany). Leachates released from MPs during photoreaction were analyzed using comprehensive two-dimensional gas chromatography coupled with time-of-flight mass spectrometry (GC×GC–TOF MS, 8890B-7250B, Agilent, USA) and atomic absorption spectrophotometry (AAS, M6, Thermo, USA). The complete analysis and data processing methods are provided in the Supplementary Material (cf. Text S2).

2.5. Computational details

All calculations were performed through ORCA 6.0 software, the B3LYP exchange-correlation functional and the 6–311 G(d) basis set were employed [28,30,4,47,54,62]. Moreover, D3(Becke–Johnson) dispersion correction was applied, and implicit solvation effects were included via the conductor-like polarizable continuum model (CPCM) with a dielectric constant of 80.4 [14,15,3]. PS degradation mainly follows a free radical mechanism, with the bond dissociation energy (BDE) approximating the reaction barrier [19–21]. BDE was calculated by:

BDE = E (Products) + E_{ZP} (Products) – E (Reactant) – E_{ZP} (Reactant)

where E is the total energy and E_{ZP} the zero-point (ZP) energy corrections [22]. The basis set superposition error (BSSE) was corrected using the counterpoise method and included in BDE [5]. The frontier orbitals, highest occupied molecular orbital (HOMO) and lowest unoccupied molecular orbital (LUMO), were visualized using Vesta software with an isosurface value of 0.005 [44].

3. Results and discussion

3.1. Impact of pigment addition on microplastics' structure

The cadmium pigment was dispersed into the polymer matrix via injection molding. This process involved heating the polymer to a molten state, uniformly blending it with pigment powder, followed by natural cooling. The cadmium pigments exhibited thermal stability exceeding 300 °C, maintaining their structural integrity during the injection molding process [12]. The morphologies of the colored microplastics synthesized from three polymer types (i.e., CdSSe-PS-MPs, CdSSe-PP-MPs, and CdSSe-PE-MPs) were characterized by SEM (Fig. S5). Micrographs revealed that injection molding enabled relatively uniform dispersion of pigment particles within the polymer matrix. However, some pigment particles located at the microplastic surfaces remained potentially exposed to the environment. These observations align with our previous findings on commercial colored PP plastic pellets [34]. Nonetheless, the injection molding machine effectively minimized oxidative polymer degradation during melting and we expect it to preserve the surface chemical structures, or at least to avoid significant alterations. To verify this, FTIR spectra of polymers and CdSSe-MPs are presented in Fig. S10, with the main absorption bands corresponding to functional groups detailed in Tables S4-S6. For both CdSSe-PS-MPs and CdSSe-PP-MPs, the FTIR spectra showed no new absorption peaks after pigment incorporation, with only marginal intensity increases of existing peaks. However, the FTIR spectrum of CdSSe-PE-MPs exhibited enhanced absorption at 1102 cm^{-1}, corresponding to C–O bond stretching vibrations, which indicates oxidation of PE during injection molding [6]. The observed oxidation likely arises from the elevated processing temperatures required to achieve optimal melt flow in PE, reflecting its higher melting point relative to PS and PP. In general, these findings suggested that injection molding did not strongly alter the surface chemistry of these three polymers, ensuring the validity of the following experiments.

3.2. Cadmium pigment promotes the photodegradation of colored microplastics

3.2.1. TOC release

Solar irradiation induces photodegradation of various microplastics, generating organic carbon as degradation products [58]. To analyze the short-term photodegradation kinetics of three CdSSe-MPs in aqueous systems, the changes in total organic carbon (TOC) concentration of CdSSe-PS-MPs, CdSSe-PP-MPs, and CdSSe-PE-MPs containing 0–30 % pigment were monitored under 8-h simulated sunlight irradiation (Fig. 1a-c). These pigment-embedded MPs are hereafter referred to as x %CdSSe-MP (x = 0, 10, 20 and 30) for simplicity. The TOC release

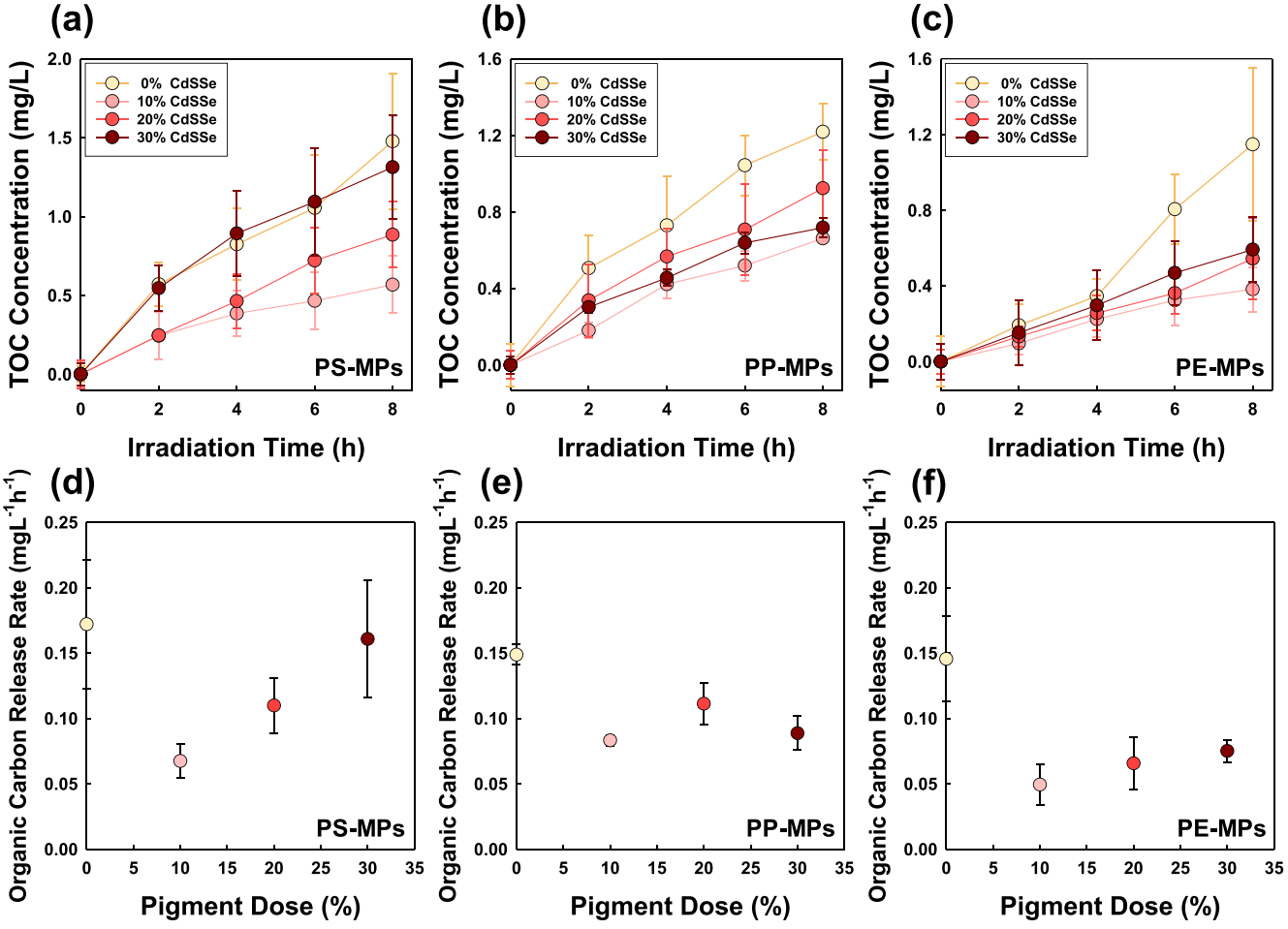

Fig. 1. (a-c) Organic carbon release kinetics and (d-f) initial organic carbon release rates of PS-MPs, PP-MPs, and PE-MPs containing 0–30 % commercial cadmium pigment during 8-h simulated sunlight irradiation. Error bars represent mean ± standard deviation (n = 3).

kinetics of the three CdSSe-MPs were analyzed by linear regression over an 8-h period, and the initial TOC release rates were determined from the slope at t→0 (r = dC(t)/dt) (Fig. 1d-f) [34]. All regressions showed good linear fits ($R^2 > 0.910$). As shown in Fig. 1, the initial TOC release is jointly influenced by both the polymer type and the dosage of cadmium pigment, with PS uniquely displaying marked sensitivity to the pigment addition. To illustrate the effect more clearly, 10 %CdSSe-MPs was first examined. The introduction of pigment into microplastics will reduce the photodegradation rate due to its ability to block the incident light. Fig. 1a shows that the TOC release of 10 %CdSSe-PS-MPs after 8-h irradiation represents only 38 % of that from unpigmented white PS-MPs. Similarly, 10 %CdSSe-PP-MPs exhibited a TOC release of 54 % compared to white PP-MPs, while 10 %CdSSe-PE-MPs released only 33 % of that from white PE-MPs (Figs. 1b and 1c). The raw TOC values used to calculate these percentages are provided in Table S3. This finding is consistent with earlier studies, as Liu et al. previously reported that iron red pigment could reduce the photodegradation rate of PP microplastics through the light-shielding effect and the competition with photogenerated transient intermediates [36].

However, when the dose of cadmium pigment increased, three types of MPs exhibit different photodegradation kinetic behaviors. In PS matrix, cadmium pigment significantly promoted the photodegradation of colored microplastics. The TOC release from 30 %CdSSe-PS-MPs after 8-h of irradiation reached 1.31 mg/L, representing a 2.31-fold increase compared to samples with 10 %CdSSe-PS-MPs. In addition, the initial TOC release rate of 30 %CdSSe-PS-MPs reached 0.161 mg/(L·h). This is almost the same level as unpigmented PS-MPs (0.172 mg/(L·h)). Extending the irradiation time to 180-h, 0 %, 10 %, and 30 %CdSSe-PS-MPs still followed this trend (Fig. S4). In contrast, cadmium pigment exhibited a weaker effect on PE-MPs and PP-MPs photodegradation. For 30 %CdSSe-PE-MPs, the TOC release after 8-h irradiation represented a 1.55-fold increase over the 10 %CdSSe-PE-MPs, and the initial TOC release rate was only 51 % of that of the unpigmented PE-MPs. For PP-MPs, increasing pigment content initially enhanced but subsequently reduced the photodegradation rate of CdSSe-PP-MPs. The TOC release amount and rate of 30 %CdSSe-PP-MPs were statistically comparable to those of the 10 %CdSSe-PP-MPs. The data to calculate the percentages for PE and PP are given in Table S3.

The three types of MPs exhibit distinct responses to cadmium pigment, primarily due to antagonistic regulation between light-shielding effects and pigment-induced photodegradation promotion. The light-shielding effect primarily correlates with pigment content per unit area. Under identical pigment dosage and particle size, this effect exhibits consistent inhibition levels on the photoreactivity of all three

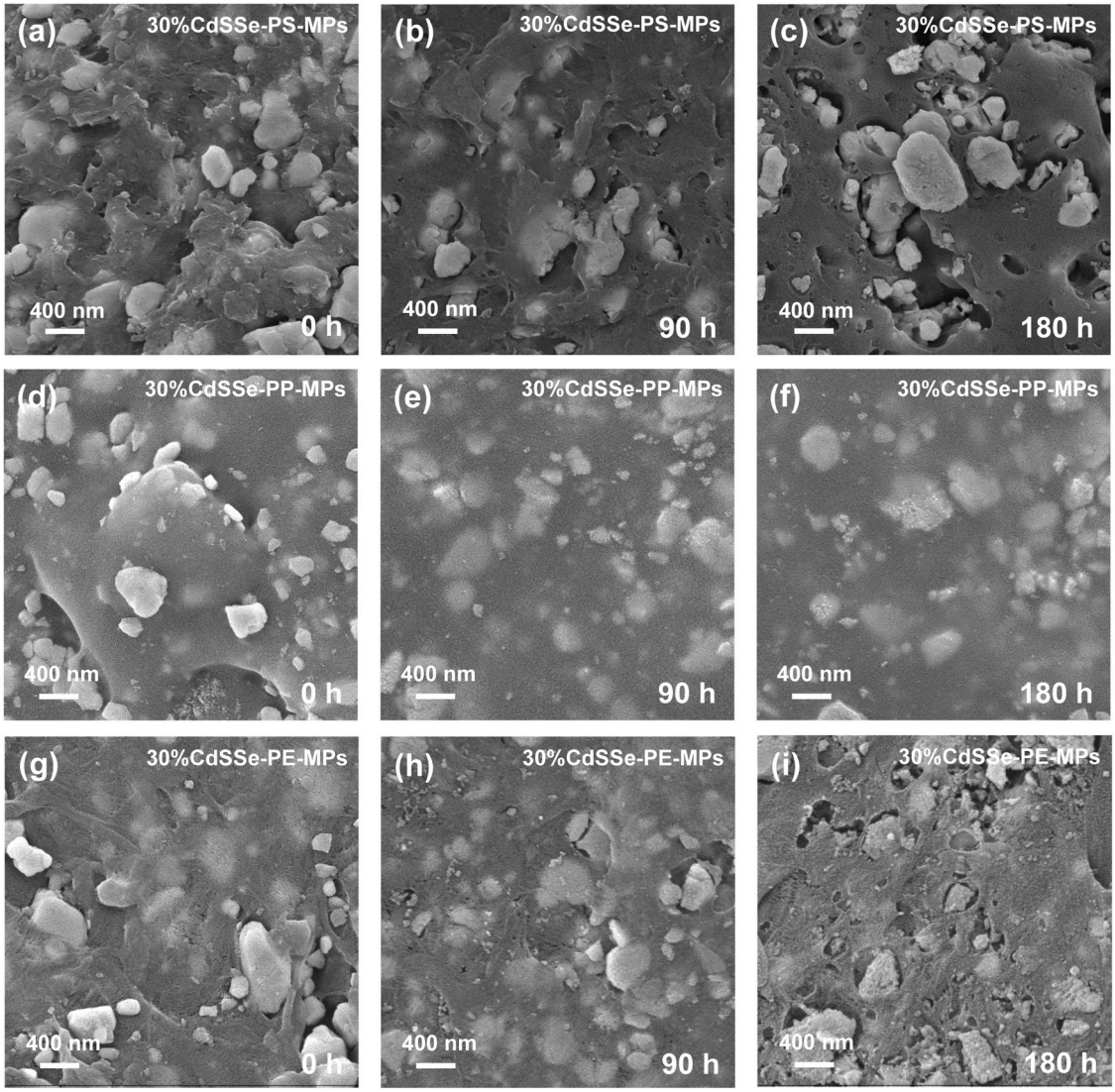

Fig. 2. SEM micrographs of (a-c) CdSSe-PS-MPs, (d-f) CdSSe-PP-MPs, and (g-i) CdSSe-PE-MPs with 30 % pigment content after 0-h, 90-h, and 180-h of simulated sunlight irradiation.

MP types. Meanwhile, the cadmium pigment exhibits intrinsic photochemical activity, generating reactive species under sunlight irradiation [33]. These reactive species may participate in polymer photoreactions, thereby promoting MPs photodegradation. The specific degradation pathways vary among different polymers, as does their susceptibility to cadmium pigment influence. Obviously, the cadmium pigment exhibits a more pronounced promoting effect on the photodegradation of the PS matrix compared to the PE and PP matrices.

3.2.2. Surface morphological evolution

Surface morphological changes of three CdSSe-MPs containing 0–30 % pigment were examined by SEM before and after 90-h and 180-h irradiation, with representative micrographs presented in Figs. 2 and S7-S9. For microplastics containing 10 % and 20 % pigment, progressive sunlight irradiation led to distinct surface evolution behaviors among different polymers. In PS-MPs and PE-MPs, exposed pigment particles on the surface gradually disappeared with irradiation time, while pores developed on the polymer surface and pigment particles from the interior became increasingly exposed. In contrast, PP-MPs did not exhibit the formation of obvious pores. These trends were even more pronounced in the 30 % pigment-containing group, as shown in Fig. 2. Prior to irradiation, all three pigmented polymers exhibited smooth surfaces with the majority of cadmium pigment particles (<600 nm) embedded within the polymer matrix, while a limited number of particles were exposed on the surface (Figs. 2a, 2d and 2g). Following 90-h irradiation, microcracks induced by photodegradation appeared on all polymer surfaces. In Figs. 2b, 2e and 2h, for pigment particles exposed on the surface, all three samples showed a significant reduction, with CdSSe-PP-MPs even exhibiting the complete disappearance. In contrast, pigment particles encapsulated within the polymers remained intact. These results agree with our previous findings that (1) only exposed particles undergo photo-dissolution through contact with water and oxygen, and (2) the polymer matrix acts as a physical barrier that temporarily protects encapsulated particles from dissolution [34].

After 180-h irradiation, all three types of CdSSe-MPs exhibited progressive surface morphological alterations with varying severity. Among them, CdSSe-PS-MPs and CdSSe-PE-MPs developed more pronounced microcracks along with apparent pore formation (Figs. 2c and 2i). Their morphologies were compared with those of the corresponding unpigmented MPs (0 % pigment content) after 180-h of irradiation (Fig. S7). PE-MPs exhibited no significant surface erosion or pore formation, and PS-MPs developed micro-scale pores with significantly smaller diameters. On the other hand, Fig. 2f shows that no erosion or pore formation could be observed on CdSSe-PP-MPs, and they exhibited similar microcrack density after 180-h irradiation to that at 90-h.

In general, the morphological changes after 90- and 180-h irradiation suggest that cadmium pigment may promote the surface damage. The damage may be attributed to the alteration of the polymer's mechanical properties due to the pigment incorporation during the injection molding process [39]. Alternatively, it could result from selective erosion of the polymer matrix induced by combined effects of pigment detachment and photooxidative degradation, ultimately resulting in irreversible surface damage. Furthermore, pigment incorporation was found to modify the mechanical properties of microplastics compared with those of the corresponding pristine polymers. To be specific, Ainali et al. reported that PP exhibits more brittle behavior than PE under UV irradiation [1]. However, comparing Fig. 2i with 2 f, PE has more brittle characteristics than PP. Meanwhile, the impact of cadmium pigment on the photodegradation of PP-MPs is lower than that of PE-MPs as Fig. 1 illustrates. Therefore, it can be concluded that the pigment can influence the surface physico-chemical properties of the polymers, with a pronounced impact on morphological evolution.

3.2.3. Surface Oxygen Content

To further investigate the chemical impact of the pigment on CdSSe-MPs, their oxidation degree was characterized using FTIR and XPS. In FTIR spectroscopy, the IR light typically penetrates several hundred nanometers, allowing the characterization of functional group variations beneath the surface. In contrast, XPS probes a depth of about 3–6 nm and is particularly sensitive to the chemical states of surface atoms [38]. Fig. S11 and Fig. 3a-c present that the FTIR spectra of unpigmented and 30 % pigment-containing MPs after exposure to simulated sunlight for 0-h, 90-h, and 180-h, respectively. The assignment of major characteristic peaks in the FTIR spectra for each microplastic sample are provided in Tables S4-S6. Fig. 3d-f present the C/O ratios obtained by XPS of unpigmented and 30 % pigmented MPs after simulated sunlight irradiation. The surface atomic percentages, along with the high-resolution C1s spectra, are presented in Table S7 and Figs. S13-S15, respectively.

As the photoreaction proceeds, the FTIR spectrum of unpigmented PS-MPs (Fig. S11a) and 30 %CdSSe-PS-MPs (Fig. 3a) exhibited increasing intensities of the broad peak at 3400 cm^{-1} (–OH stretching) and the sharp peak at 1735 cm^{-1} (C═O stretching). It indicates the formation of C–OH and C═O functional groups during irradiation for both pigmented and unpigmented PS-MPs [29,55]. After 180-h of irradiation, the carbonyl index (CI) and hydroxyl index (HI) of unpigmented PS-MPs increased to 2.09 and 5.81 times their initial values, respectively. In contrast, the CI and HI of 30 %CdSSe-PS-MPs rose much more markedly, reaching 7.15- and 7.53-fold of their initial values, respectively (Figs. S12a and S12b). The higher formation of hydroxyl and carbonyl functional groups in 30 %CdSSe-PS-MPs confirms a greater degree of surface oxidation compared with unpigmented PS-MPs. XPS analysis further determined the variation in surface oxygen content for the two samples (Fig. 3d). After the same irradiation period (90- and 180-h), the atomic C/O ratio of 30 %CdSSe-PS-MPs was lower than that of white PS-MPs, demonstrating a higher degree of surface oxidation. In the high-resolution C 1 s spectra of both PS-MPs, the component corresponding to hydroxyl carbon (C–OH, 286.3 eV) increased significantly after 180-h irradiation (Fig. S13), which is consistent with the FTIR observations. In the C1s spectra, the hydroxyl carbon (C–OH, 286.3 eV) component showed a significant increase after 180-h irradiation, consistent with FTIR detection (Fig. S13). Although an additional carbonyl carbon component (C═O, 288.8 eV) was detected in white PS-MPs, 30 %CdSSe-PS-MPs exhibited higher oxygen content and greater abundance of hydroxyl carbon. Namely, the incorporation of cadmium pigment intensifies the surface oxidation of PS-MPs, which is in agreement with the SEM morphological characterization showing an increased number of small holes.

Moreover, the cadmium pigment also intensified the oxidation of PP- and PE-MPs during irradiation. With prolonged simulated solar irradiation, the FTIR spectra of 30 %CdSSe-PP-MPs showed progressively intensified peaks at 3400 cm^{-1} (O–H stretching) and 1735 cm^{-1} (C═O stretching), indicating gradual formation of C–OH and C═O functional groups (Fig. 3b). By comparison, peak enhancement was less pronounced in white PP-MPs (Fig. S11b). After 180-h of irradiation, the CI of 30 %CdSSe-PP-MPs increased by 32.3 % relative to its initial value, slightly higher than that of white PP-MPs (26.5 %). In addition, the HI of 30 %CdSSe-PP-MPs increased markedly by 125 %, whereas no increase was observed for white PP-MPs (Figs. S12c and S12d). XPS analysis revealed that 30 %CdSSe-PP-MPs exhibited lower C/O atomic ratios after 90- and 180-h irradiation compared to white PP-MPs, along with higher abundance of hydroxyl carbon and carbonyl carbon in C1s spectra, indicating more severe surface oxidation in pigmented PP-MPs (Figs. 3e and S14). Meanwhile, the FTIR spectra of 30 %CdSSe-PE-MPs demonstrated that during irradiation, not only did the characteristic peaks of hydroxyl (3400 cm^{-1}) and carbonyl (1735 cm^{-1}) groups continue to intensify, but the C–O bond peak at 1102 cm^{-1} also showed significant enhancement (Fig. 3c). In contrast, white PE-MPs exhibited minimal intensity changes in these three characteristic peaks (Fig. S11c). The CI and HI of 30 % CdSSe-PE-MPs increased to 2.32 and 1.58 times their initial values after 180-h of irradiation, respectively, both markedly higher than those of white PE-MPs. By comparison, the CI

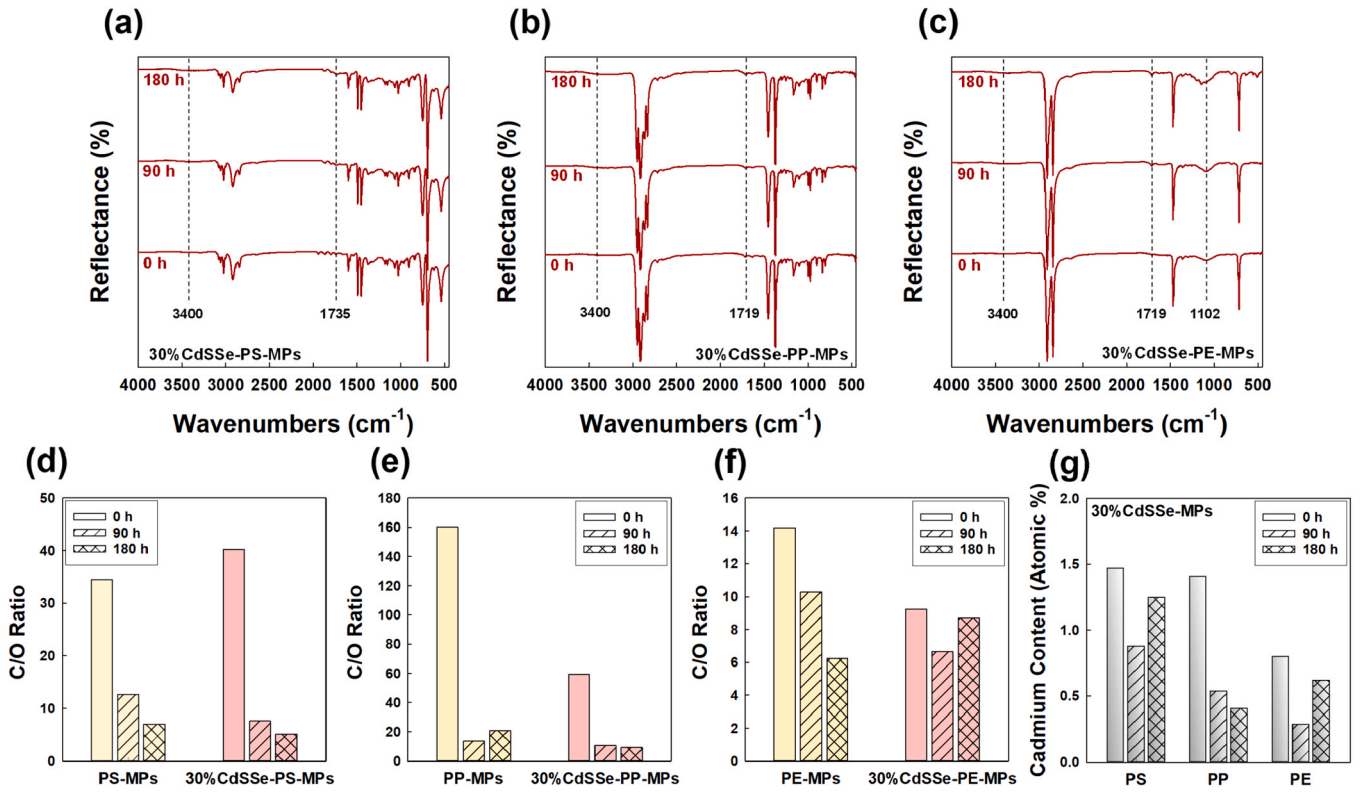

Fig. 3. FTIR spectra and C/O ratio of (a, d) PS-MPs, (b, e) PP-MPs, and (c, f) PE-MPs with 30 % pigment content after 0-h, 90-h, and 180-h of simulated sunlight irradiation. (g) Cadmium content of three 30 %CdSSe-MPs after 0-h, 90-h, and 180-h of simulated sunlight irradiation.

of white PE-MPs remained nearly unchanged, and its HI increased only to 1.44 times the initial value (Figs. S12e and S12f). These results indicate that the cadmium pigment significantly promotes C–O bond formation of PE-MPs. However, for CdSSe-PE-MPs, XPS analysis does not fully align with the FTIR observations. XPS spectra (Fig. 3f) reveal that the atomic ratio C/O of 30 %CdSSe-PE-MPs was significantly lower than that of white PE-MPs after 90-h irradiation, whereas it rebounded after 180-h irradiation. Meanwhile, no strong signal appeared at 286.3 eV (corresponding to C–O carbon) in the C1s spectra of 30 % CdSSe-PE-MPs after 180-h irradiation (Fig. S15). The discrepancy between FTIR and XPS results for PE-MPs is likely caused by C–O bond formation in deeper damaged layers, considering the different probing depths of these two techniques.

3.2.4. *Crystallinity*

XRD was used to examine changes in the crystallinity of colored microplastics during photoreaction. Prior to irradiation, the crystallinity of 30 %CdSSe-PP-MPs was lower than that of unpigmented PP-MPs (Fig. S16). This reduction is likely attributable to the dispersion of pigments within the PP matrix, which introduces spatial barriers that restrict chain-segment mobility and hinder ordered packing. With continued irradiation, the crystallinity of both PP-MPs and 30 %CdSSe-PP-MPs gradually increased. This trend can be ascribed to chain scission in amorphous regions, followed by molecular rearrangement into more ordered crystalline microstructures [16,59]. After 180-h of irradiation, the crystallinity of unpigmented PP-MPs increased from 59.1 % to 69.9 % (an increase of 18.2 %), while that of 30 %CdSSe-PP-MPs increased only from 53.0 % to 57.1 % (an increase of 7.66 %). These results indicate that the presence of cadmium pigments suppresses crystallization in PP during photoreaction.

In contrast to PP, the crystallinity of PE decreased after irradiation, a trend recognized as an indicator of polymer aging in previous studies [31]. After 180-h of irradiation, the crystallinity of unpigmented PE-MPs decreased from 67.2 % to 58.0 %, while that of 30 %CdSSe-PE-MPs decreased from 67.6 % to 57.2 %. These comparable reductions indicate that cadmium pigments exert little influence on the crystallization behavior of PE-MPs. For PS, which is amorphous, crystallinity was not evaluated. From a mechanistic perspective, changes in crystallinity reorganize surface molecular chains and thereby modify particle surface properties. The distinct crystallinity evolution observed for PP and PE may help explain their different sensitivities to pigment-induced photoactivation. In PP-MPs, increased crystallinity can act as a physical barrier to pigment-generated reactive species, suppressing polymer photodegradation [37].

In general, cadmium pigments intensify the photodegradation of PS, PP, and PE microplastics, resulting in surface damage and oxidation. Among these polymers, PS shows a notably stronger response to cadmium pigments in terms of small-molecule carbon release and surface erosion, which are indicated by their TOC release rate and the pore formation as SEM characterized. The small-molecule carbon release may arise from the polymer degradation products or leached additives. This pronounced sensitivity of PS might be partially attributed to its aromatic phenyl groups, which could interact differently with photogenerated reactive species compared to the aliphatic backbones of PP and PE. Although PS exhibits a higher TOC release and more severe surface damage, both XPS and FTIR results show comparable surface oxygen level among the three polymers. This may result from the enhanced chain scission and the detachment of aromatic rings in PS degradation pathways, leading to higher small-molecule release without proportionally increasing the surface oxygen content.

Another important observation is the positive correlation between pigment-promoted polymer photodegradation and pigment photodissolution. In well-illuminated aquatic environments, the photodissolution of cadmium pigments releases toxic Cd^{2+} ions [33,34]. The short-term leaching kinetics of Cd^{2+} from colored microplastics with different pigment host were evaluated during 8-h of irradiation (as shown in Fig. S17). Cd^{2+} leaching was observed for all samples under light exposure, with the released amount increasing as pigment host

increased. At the early stage of photoreaction, the polymer matrix exhibited no appreciable structural changes, and Cd^{2+} release showed a good linear relationship with irradiation time ($R^2 > 0.96$). Linear regression of the kinetic curves yielded initial release rates, which increased systematically with pigment content (Table S8). These findings demonstrate that Cd^{2+} is released from cadmium-pigmented microplastics upon light irradiation, and that both the release amount and rate are positively correlated with pigment loading, consistent with previous reports [34]. As depicted in Fig. 3g and 1d-f, the Cd^{2+} content detected and the TOC release rate of all three CdSSe-MPs follow the same trend, highlighting this correlation. The altered photodissolution process is explained by the surface morphological evolution induced by photodegradation, which exposes more pigment particles to irradiation. Fig. 3g shows that the surface Cd content of the three polymers decreases significantly after 90-h of irradiation due to the extensive photo-dissolution of pigment particles. After 180-h, severe surface damage is observed on 30 %CdSSe-PS-MPs and 30 %CdSSe-PE-MPs, resulting in more pigment particles being exposed and a subsequent increase in the Cd atomic percentage. In contrast, the surface of 30 % CdSSe-PP-MPs remains largely intact, and its Cd atomic percentage continues to decline. The interplay, where photodegradation-induced surface damage promotes pigment photodissolution, results in persistent Cd^{2+} release, potentially amplifying the ecotoxicity and environmental risks associated with pigment-containing microplastics. Furthermore, this observation shifts our focus to the pigment photodissolution as a key factor in explaining the photodegradation mechanism of CdSSe-MPs.

3.3. Degradation Mechanism of colored microplastics

Based on our previous studies, the cadmium pigment is mainly composed of CdS_xSe_{1-x}, in which the S/Se molar ratio is 1.9 ± 0.1. It is a semiconductor with a band gap of 2.08 V and can be photoexcited by light with wavelengths below 596 nm. The conduction band potential of this pigment is −1.06 V (SHE), and the valence band potential is 1.02 V (SHE). Upon light irradiation, the cadmium pigment becomes photoexcited, and the photogenerated holes can oxidize the pigment lattice. This process leads to the release of Cd^{2+}, while S and Se are simultaneously oxidized to SO_4^{2-} and SeO_4^{2-}, respectively (Fig. 5b). The pigment-induced differences in photodegradation rates among polymers may arise from changes in the underlying degradation pathways caused by the pigments. As discussed above, among the polymers investigated, PS exhibited the strongest response to pigment presence and is therefore discussed here in detail. Conventionally, polymer photodegradation is initiated by UV-induced bond cleavage, typically involves the generation of free radicals, as illustrated in Path1 (Fig. 5c) [63,67]. However, for colored microplastics, the semiconductor property of the cadmium pigment, introduces additional complexity. Upon light irradiation (λ<596 nm), CdSSe generate photo-induced electrons and holes (Fig. 5a), which initiate redox reactions producing $O_2^{\bullet-}$ and •OH free radicals. In addition, the photodissolution of the pigment releases protons (Fig. 5b), which also exhibit photoinduced activity [66]. The microenvironment, with high concentration of these photo-induced reactive species on the polymer surface, may significantly influence or even alter the degradation pathways of adjacent polymer regions. Previous studies have shown that colored microplastics display significantly enhanced photochemical activity compared to their uncolored counterparts, due to their ability to generate reactive oxygen species (ROS), which facilitate the efficient degradation of contaminants [11,43,63,66,72]. In this work, we focus on the degradation of plastics themselves instead of the pollutants. We observed that PS-, PP-, and PE-MPs embedded with cadmium pigments exhibited distinct degradation rates when exposed to an aquatic environment. These differences in degradation are hypothesized to stem from the chemical nature and reactivity of pigment-induced intermediates, especially considering that the structure of polymers strongly influences their interaction with such reactive species.

Among the tested microplastics, the pronounced sensitivity of PS to pigment-induced changes suggests that protons may act as critical species driving its accelerated degradation. Due to the presence of conjugated benzene rings, PS appears to be particularly susceptible to proton attack, which are known to undergo acid-catalyzed degradation [2,68]. As previously reported, under acidic conditions, BDEs of PS are reported to decrease significantly, especially for aromatic C–C bonds in branched chains [18]. This suggests that the protons released during the pigment photodissolution may attack the phenyl groups of PS, making the polymer more prone to cleavage and ultimately accelerating the degradation process [21]. To further elucidate the underlying mechanism, we performed DFT calculations on the PS···H_3O^+ complex and analyzed its frontier molecular orbitals (HOMO and LUMO), as shown in Fig. 4b. LUMO reveals that the interactions between the phenyl functional groups and H_3O^+ could enhance the electron delocalization. This enables the protonation at benzylic positions and the formation of carbocation, which is depicted as structure ⑥ in Fig. 5c. Compared with PS, aliphatic PP and PE shows no notable interaction with H_3O^+, as evidenced by the absence of frontier orbital overlap in Fig. 4b. This result corresponds to the limited effect of cadmium pigments on their degradation behavior. This observation is further supported by Hirshfeld charge analysis of the polymer–H_3O^+ complexes. The amounts of charge transfer between the two fragments are 0.39, 0.25, and 0.19 e for PS-, PP-, and PE-H_3O^+, respectively, providing quantitative evidence for differences in electronic coupling. The larger charge transfer observed for PS can be attributed to the presence of conjugated benzene rings. In contrast, the smallest charge transfer in PE is likely caused by steric hindrance from the ethyl substituents, which restricts the approach of H_3O^+ to the polymer backbone. The degradation pathways for PS are summarized in Fig. 5c. Path1 corresponds to the well-studied photooxidation process, while Path2 follows an acid-catalyzed mechanism that was reported in detail by Huang et al. Huang et al., [21,63,67].

Additionally, given the presence of photo-induced electron generated by the pigment, we also propose an alternative mechanism designated as Path3. Following the formation of the carbocation intermediate, the reaction may proceed along Path2 and Path 3, in which a photo-induced electron is donated to the carbocation, yielding a carbon-centered radical (structure ⑦). This radical further evolves into a radical bearing an alkene moiety (structure ⑨). It could further react with oxygen to form ROS, thereby propagating the degradation process as Path1. FTIR and XPS analyses indicated an increase in C–OH and C═O functional groups in irradiated CdSSe-PS-MPs, providing additional evidence for the occurrence of oxidation reactions. While the photooxidation Path1 has been extensively studied, our attention is directed toward the role of protons in Path2 and Path3, as CdSSe may serve as a catalyst that facilitates proton generation and electron transfer and provides an active surface for the reactions to occur [43,63,66,68]. Furthermore, the presence of alkene-containing compounds in the GC-MS analysis strongly supports the validity of Path2 and Path3, both of which involve the formation of C═C bonds. In the photodegradation products of PS-MPs with 10 % pigment loading, six alkene compounds were identified (Fig. S18), none of which were observed in the degradation products of unpigmented PS-MPs. To demonstrate the plausibility of the newly proposed Path 3 in this work, we constructed an energy barrier profile for the degradation process based on DFT calculations (Fig. 6). The profile shows a stepwise decrease along the degradation suggests that this pathway is thermodynamically favorable. The branching point between Path2 and Path3 lies in whether the carbocation can capture the photo-induced electron. In Fig. 6, Steps 2, 5, and 8 involve electron transfer processes leading from carbocations to carbon-centered radicals. Their Gibbs free energy changes (ΔG) were determined via DFT calculations and were listed in Table S9. Based on the calculated ΔG values, the redox potentials versus the standard hydrogen electrode (SHE, E^0 = 4.188 V) were determined via the Gibbs–Nernst equation to be 0.30 V, −0.59 V, and 0.20 V, respectively

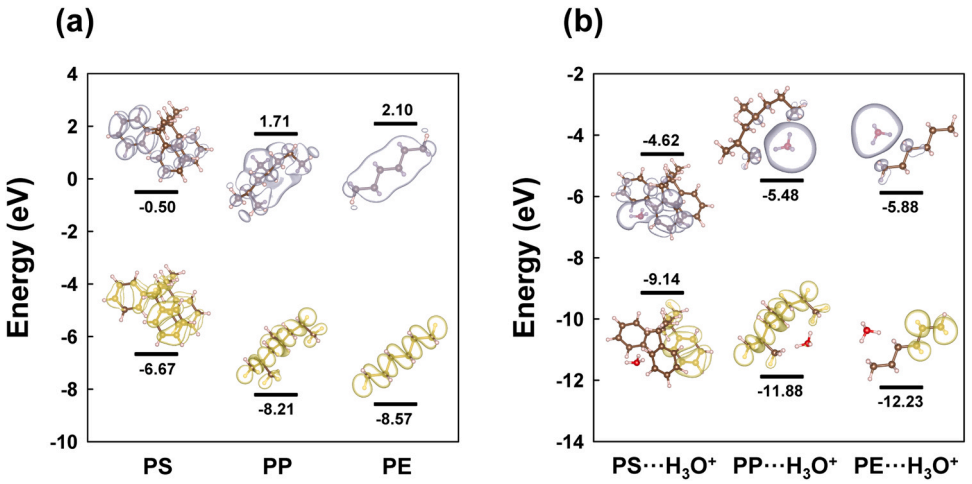

Fig. 4. Yellow HOMO and purple LUMO isosurfaces for (a) PS, PP and PE; (b) PS···H_3O^+, PP···H_3O^+ and PE···H_3O^+ complex.

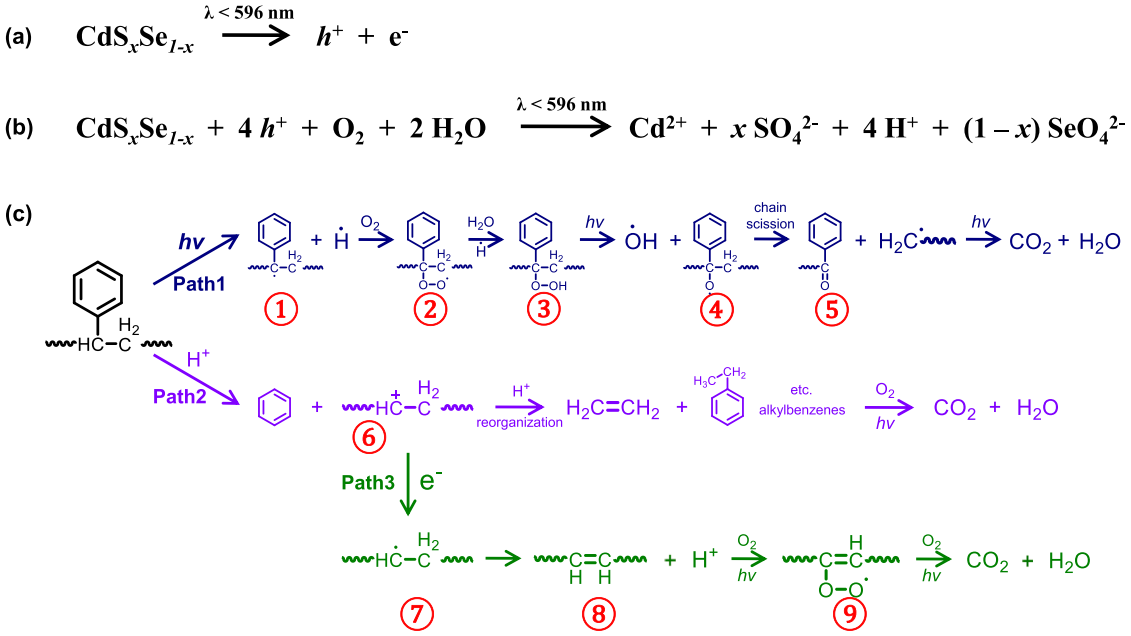

Fig. 5. (a) Photo-induced generation of electron–hole pairs by CdSSe; (b) Photo-dissolution of CdSSe leading to the release of Cd^{2+} and protons; (c) The degradation mechanisms of PS-MPs including blue Path1—photooxidation reactions, purple Path2—acid-catalyzed degradation pathways and green Path3—acid-induced photo-degradation scheme.

[53]. The calculated redox potentials are all more positive than the conduction band potential of CdSSe (-1.06 V versus SHE), indicating that the photogenerated electrons possess sufficient reducing power to drive these reduction steps [41]. Given that some carbocation intermediates exhibit redox potentials comparable to or lower than that of oxygen (-0.16 V versus SHE), a competitive electron transfer may occur under irradiation, allowing both ROS formation and Path3 to co-exist [32]. Taken together, the degradation of PS-MPs involves multiple pathways (Fig. 5c): classical photooxidation (Path1), proton-mediated acid-catalyzed degradation (Path2), and photo-induced electron-driven reduction of carbocations (Path3). It highlights the mechanistic complexity arising from the microenvironment, where a pool of reactive species (including localized protons, electrons, and ROS) is enriched near the polymer surface by the pigment.

3.4. *Cadmium pigment intensify additive leaching from microplastics*

Cadmium pigments further promote the leaching of endogenous additives from microplastics. GC×GC–TOF MS was employed to semi-quantitatively screen low-molecular-weight organic compounds in leachates from both pigmented and unpigmented MPs after 90-h of simulated sunlight irradiation. Unpigmented microplastics were used as controls alongside experimental groups with gradient pigment loadings. Characteristic ion peaks were identified, and the corresponding peak areas were integrated. Considering the potential occurrence of secondary reactions under prolonged high-intensity irradiation, absolute quantification of low-molecular-weight products was not performed. Instead, ratios of integrated peak areas were used to represent the relative abundances of compounds released from pigmented versus unpigmented microplastics. Molecular species exhibiting more than a 100-fold higher relative concentration in CdSSe-MP leachates than in unpigmented MPs were identified as characteristic leaching products. Detailed compound identification criteria, including retention times, retention indices, characteristic ion fragments, and spectral match factors, are provided in Table S10. These findings indicate that pigment presence substantially enhances their release. The structures of these

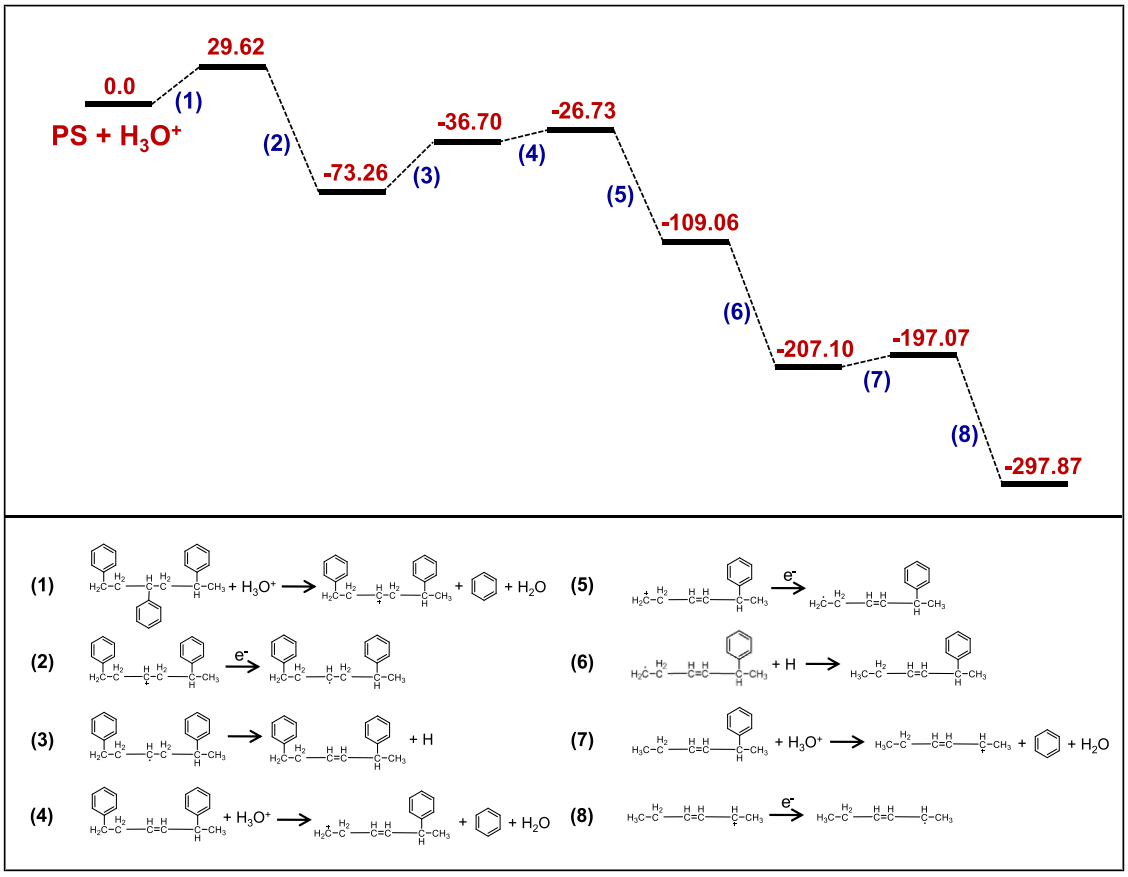

Fig. 6. Scheme of reaction energy barriers for Path3, including (1)-(8) reactions. Energy values are in kcal/mol.

characteristic leaching products were confirmed by matching mass spectral fragmentation, retention times, retention indices, and ion masses with database standards (Table S10). Notably, the characteristic leaching products detected in the leachate do not completely match the additives identified in the plastic raw materials (Table S1). The identification of the possible origins of these characteristic leaching products is largely based on reports in previous research (as shown in Table S11). A total of 19 characteristic leaching products were identified in the CdSSe-PS-MPs system (Table S11). Among them, 14 were classified as plastic additives and their derivatives, while the remaining 5 could originate from either additive intermediates or polymer photodegradation products. The additional leaching of additives is primarily attributed to the accelerated chain scission of PS polymers induced by cadmium pigment. This degradation process not only reduces the diffusion resistance of additives within PS-MPs, but also generates abundant surface pores, thereby facilitating the transboundary migration of additives into the aqueous phase [8]. In the CdSSe-PP-MPs system, a total of 23 characteristic leaching products were identified. Among them, 19 compounds are definitively characterized as plastic additives and their derivatives, while the remaining 4 may originate from multiple potential sources. Although cadmium pigments do not markedly promote the photodegradation of PP-MPs, they still significantly intensify additive leaching during photochemical reactions. This observation may be associated with the crystalline state of the polymer. To be specific, PS is an amorphous glassy polymer exhibiting high rigidity, thereby conferring substantial resistance to additive leaching [13]. In contrast, PP typically exhibits a semi-crystalline morphology with rubbery domains. The rubbery phase exhibits greater molecular disorder and expanded free volume regions, thereby promoting additive leaching [73]. XRD analysis revealed that the incorporation of cadmium pigment significantly reduced the crystallinity of PP-MPs. This indicates an increased proportion of amorphous regions in PP-MPs, reducing migration resistance and significantly enhancing leachate release. PE-MPs exhibit higher crystallinity and demonstrate minimal susceptibility to cadmium pigment, resulting in significantly hindered additive migration and leaching (Fig. S19). Only one characteristic leaching product was detected in the CdSSe-PE-MPs system, which was identified as an organophosphate derivative.

Notably, among the characteristic leaching products from all three polymers, multiple persistent and hazardous compounds were identified. Particularly concerning are the phthalate esters (PAEs) - including diethyl phthalate (DEP), diisobutyl phthalate (DIBP), and dibutyl phthalate (DBP) - which represent a class of endocrine disrupting chemicals. These compounds have been scientifically demonstrated to cause severe adverse effects on human respiratory, reproductive, and endocrine systems, while exhibiting significant environmental persistence [10,71]. The organophosphate flame retardant tributyl phosphate (TBP) has been identified as an emerging persistent organic pollutant (POP) due to its documented bioaccumulation potential in biota and long-term disruptive effects on avian endocrine and reproductive systems [10,45]. The heterocyclic aromatic compound benzothiazole has been demonstrated to exhibit embryotoxic effects in both fish and mammalian species [7]. Furthermore, the Occupational Safety and Health Administration (OSHA) database analysis confirmed the presence of 7 established animal carcinogens, 3 suspected human carcinogens, and 1 unclassifiable human carcinogen among the characteristic leaching products (Table S11) [50]. This finding provides definitive evidence that cadmium pigment-colored microplastics pose elevated environmental risks and potential health threats.

4. Conclusion

This study demonstrates that cadmium pigments significantly reshape the photodegradation behavior of PS, PP, and PE microplastics. In well-illuminated aquatic environments, the effect of cadmium pigments on the photodegradation of microplastics strongly depends on the polymer structure. Experimental observations from TOC release, SEM, FTIR, and XPS analyses reveal that pigment incorporation accelerates polymer chain scission and surface oxidation, with PS showing the strongest response. Upon light irradiation, the pigments can generate photo-induced electrons, holes, protons, and various reactive radicals, which can interact with polymers and participate in the reactions, leading to more complex degradation pathways. Proton attack on phenyl groups in PS enables carbocation and radical-mediated pathways, as confirmed by DFT calculations. These findings indicate that pigment–polymer interactions critically influence microplastic degradation. Moreover, pigment addition enhances the leaching of hazardous additives, amplifying ecological risks. Together, these results highlight the dual role of pigments in accelerating polymer weathering and mobilizing toxic species. These findings also underscore the urgent need to account for pigment–polymer interactions in environmental assessments. To mitigate risks from these microplastics, future work should focus on structural modifications of both pigments and polymer matrices, as their combined properties jointly influence fragmentation and degradation behavior. In parallel, the development of safer alternatives is essential for source control, which ultimately represents the most sustainable solution to this environmental issue.

Environmental implications

Cadmium pigments accelerate microplastic photodegradation, intensifying fragmentation and additive leaching that heighten ecological toxicity. Considering that cadmium-colored plastics remain indispensable in certain applications, limiting pigment photodissolution and developing safer alternatives represents a more effective long-term approach to addressing their environmental impacts.

CRediT authorship contribution statement

Yuxuan Yao: Writing – review & editing, Methodology, Conceptualization. **Harald Oberhofer:** Writing – review & editing, Resources. **Xiaolei Qu:** Writing – review & editing, Resources. **Huiting Liu:** Writing – original draft, Methodology, Investigation, Funding acquisition. **Kexin He:** Writing – review & editing, Resources. **Shijia Xu:** Visualization, Validation, Investigation.

Declaration of Competing Interest

The authors declare that they have no known competing financial interests or personal relationships that could have appeared to influence the work reported in this paper.

Acknowledgements

This work was supported by the National Natural Science Foundation of China (Grant 22206132). Y.Y. acknowledges the valuable discussions with Xinyou Ma. H. L. acknowledges Linzi Zuo for the GC-MS testing and analysis.

Supplementary data

Supplementary data related to this article can be found at https://XX/XXX.

Appendix A. Supporting information

Supplementary data associated with this article can be found in the online version at doi:10.1016/j.jhazmat.2026.141297.

Data Availability

Data will be made available on request.

References

[1] Ainali, N.M., Bikiaris, D.N., Lambropoulou, D.A., 2021. Aging effects on low- and high-density polyethylene, polypropylene and polystyrene under UV irradiation: An insight into decomposition mechanism by Py-GC/MS for microplastic analysis. J Anal Appl Pyrol 158, 105207. https://doi.org/10.1016/j.jaap.2021.105207.
[2] Amjad, U.-e-S., Tajjamal, A., Ul-Hamid, A., Faisal, A., Zaidi, S.A.H., Sherin, L., Mir, A., Mustafa, M., Ahmad, N., Hussain, M., Park, Y.-K., 2022. Catalytic cracking of polystyrene pyrolysis oil: Effect of Nb_2O_5 and NiO/Nb_2O_5 catalyst on the liquid product composition. Waste Manag 141, 240–250. https://doi.org/10.1016/j.wasman.2022.02.002.
[3] Barone, V., Cossi, M., 1998. Quantum calculation of molecular energies and energy gradients in solution by a conductor solvent model. J Phys Chem A 102 (11), 1995–2001. https://doi.org/10.1021/jp9716997.
[4] Becke, A.D., 1993. Density-functional thermochemistry. III. The role of exact exchange. J Chem Phys 98 (7), 5648–5652. https://doi.org/10.1063/1.464913.
[5] Boys, S.F., Bernardi, F., 1970. The calculation of small molecular interactions by the differences of separate total energies. Some procedures with reduced errors. Mol Phys 19 (4), 553–566. https://doi.org/10.1080/00268977000101561.
[6] Brandon, J., Goldstein, M., Ohman, M.D., 2016. Long-term aging and degradation of microplastic particles: Comparing in situ oceanic and experimental weathering patterns. Mar Pollut Bull 110 (1), 299–308. https://doi.org/10.1016/j.marpolbul.2016.06.048.
[7] Capolupo, M., Sørensen, L., Jayasena, K.D.R., Booth, A.M., Fabbri, E., 2020. Chemical composition and ecotoxicity of plastic and car tire rubber leachates to aquatic organisms. Water Res 169, 115270. https://doi.org/10.1016/j.watres.2019.115270.
[8] Cao, Y., Liu, Y., Guo, K., He, W., Hur, J., Guo, H., 2025. Molecular characteristics and plastic additives in dissolved organic matter derived from polystyrene microplastics: Effects of cumulative irradiation and microplastic concentrations. Water Res 282, 123641. https://doi.org/10.1016/j.watres.2025.123641.
[9] Chen, Q., Li, Y., Li, B., 2020. Is color a matter of concern during microplastic exposure to *Scenedesmus obliquus* and *Daphnia magna*? J Hazard Mater 383, 121224. https://doi.org/10.1016/j.jhazmat.2019.121224.
[10] Cong, B., Li, S., Liu, S., Mi, W., Liu, S., Zhang, Z., Xie, Z., 2022. Source and distribution of emerging and legacy persistent organic pollutants in the basins of the Eastern Indian Ocean. Environ Sci Technol 56 (7), 4199–4209. https://doi.org/10.1021/acs.est.1c08743.
[11] Fabbri, D., Carena, L., Bertone, D., Brigante, M., Passananti, M., Vione, D., 2023. Assessing the photodegradation potential of compounds derived from the photoinduced weathering of polystyrene in water. Sci Total Environ 876, 162729. https://doi.org/10.1016/j.scitotenv.2023.162729.
[12] Faulkner, E.B., Schwartz, R.J., 2009. High Performance Pigments. Wiley-VCH Verlag-GmbH, Weinheim, Germany.
[13] Fried, J.R., 2010. Polymer Science and Technology. Pearson Education Inc, Upper Saddle River, New Jersey, USA.
[14] Grimme, S., Antony, J., Ehrlich, S., Krieg, H., 2010. A consistent and accurate *ab initio* parametrization of density functional dispersion correction (DFT-D) for the 94 elements H-Pu. J Chem Phys 132 (15), 154104. https://doi.org/10.1063/1.3382344.
[15] Grimme, S., Ehrlich, S., Goerigk, L., 2011. Effect of the damping function in dispersion corrected density functional theory. J Comput Chem 32 (7), 1456–1465. https://doi.org/10.1002/jcc.21759.
[16] Gupta, A.P., Saroop, U.K., Gupta, V., 2007. Studies on the photo-oxidation of PP and PP/mLLDPE blend systems: Thermal, physicochemical, and mechanical behavior. J Appl Polym Sci 106, 917–925. https://doi.org/10.1002/app.26762.
[17] Guo, P., Ye, C., Guo, Y., Chen, Z., Zhang, Z., Zhou, C., Xiao, W., Wen, H., Wang, Y., Huang, H., Zhang, M., 2024. Visible light-induced PET degradation using red $Cd_xZn_{1-x}Se_yS_{1-y}$ quantum dots capped with two different ligands under varying pH conditions. J Environ Chem Eng 12, 112170. https://doi.org/10.1016/j.jece.2024.112170.
[18] Hernández Fernández, J.A., Prieto Palomo, J.A., Ortega-Toro, R., 2025. Application of computational studies using density functional theory (DFT) to evaluate the catalytic degradation of polystyrene. Polymers 17 (7), 923. https://doi.org/10.3390/polym17070923.
[19] Huang, J., He, C., Pan, G., Tong, H., 2016. A theoretical research on pyrolysis reactions mechanism of coumarone-contained lignin model compound. Comput Theor Chem 1091, 92–98. https://doi.org/10.1016/j.comptc.2016.07.016.
[20] Huang, J., He, C., Li, X., Pan, G., Tong, H., 2018. Theoretical studies on thermal degradation reaction mechanism of model compound of bisphenol A polycarbonate. Waste Manag 71, 181–191. https://doi.org/10.1016/j.wasman.2017.10.016.

[21] Huang, J., Cheng, X., Meng, H., Pan, G., Wang, S., Wang, D., 2020. Density functional theory study on the catalytic degradation mechanism of polystyrene. AIP Adv 10 (8), 085004. https://doi.org/10.1063/5.0013211.
[22] Huang, J., Li, X., Meng, H., Tong, H., Cai, X., Liu, J., 2020. Studies on pyrolysis mechanisms of syndiotactic polystyrene using DFT method. Chem Phys Lett 747, 137334. https://doi.org/10.1016/j.cplett.2020.137334.
[23] Imhof, H.K., Laforsch, C., Wiesheu, A.C., Schmid, J., Anger, P.M., Niessner, R., Ivleva, N.P., 2016. Pigments and plastic in limnetic ecosystems: A qualitative and quantitative study on microparticles of different size classes. Water Res 98, 64–74. https://doi.org/10.1016/j.watres.2016.03.015.
[24] Ivleva, N.P., Wiesheu, A.C., Niessner, R., 2017. Microplastic in aquatic ecosystems. Angew Chem Int Ed 56 (7), 1720–1739. https://doi.org/10.1002/ange.201606957.
[25] Klemchuk, P.P., 1983. Influence of pigments on the light stability of polymers: A critical review. Polym Photochem 3 (1), 1–27. https://doi.org/10.1016/0144-2880(83)90042-8.
[26] Koelmans, A.A., Nor, N.H.M., Hermsen, E., Kooi, M., Mintenig, S.M., de France, J., 2019. Microplastics in freshwaters and drinking water: Critical review and assessment of data quality. Water Res 155, 410–422. https://doi.org/10.1016/j.watres.2019.02.054.
[27] Koelmans, A.A., Redondo-Hasselerharm, P.E., Nor, N.H.M., de Ruijter, V.N., Mintenig, S.M., Kooi, M., 2022. Risk assessment of microplastic particles. Nat Rev Mater 7 (2), 138–152. https://doi.org/10.1038/s41578-021-00411-y.
[28] Krishnan, R., Binkley, J.S., Seeger, R., Pople, J.A., 1980. Self-consistent molecular orbital methods. XX. A basis set for correlated wave functions. J Chem Phys 72 (1), 650–654. https://doi.org/10.1063/1.438955.
[29] Lam, S.-M., Chew, K.-C., Sin, J.-C., Zeng, H., Lin, H., Li, H., Lim, J.W., Mohamed, A. R., 2022. Ameliorated photodegradation performance of polyethylene and polystyrene films incorporated with ZnO-PVP catalyst. J Environ Chem Eng 10 (3), 107594. https://doi.org/10.1016/j.jece.2022.107594.
[30] Lee, C., Yang, W., Parr, R.G., 1988. Development of the Colle-Salvetti correlation-energy formula into a functional of the electron density. Phys Rev B 37 (2), 785–789. https://doi.org/10.1103/PhysRevB.37.785.
[31] Li, M., He, L., Hsieh, L., Rong, H., Tong, M., 2023. Transport of plastic particles in natural porous media under freeze–thaw treatment: Effects of porous media property. J Hazard Mater 442, 130084. https://doi.org/10.1016/j.jhazmat.2022.130084.
[32] Li, J., Jiang, M., Zhou, H., Jin, P., Cheung, K.M.C., Chu, P.K., Yeung, K.W.K., 2019. Vanadium dioxide nanocoating induces tumor cell death through mitochondrial electron transport chain interruption. Glob Chall 3 (3), 1800058. https://doi.org/10.1002/gch2.201800058.
[33] Liu, H., Gao, H., Long, M., Fu, H., Alvarez, P.J.J., Li, Q., Zheng, S., Qu, X., Zhu, D., 2017. Sunlight promotes fast release of hazardous cadmium from widely-used commercial cadmium pigment. Environ Sci Technol 51 (12), 6877–6886. https://doi.org/10.1021/acs.est.7b00654.
[34] Liu, H., Liu, K., Fu, H., Ji, R., Qu, X., 2020. Sunlight mediated cadmium release from colored microplastics containing cadmium pigment in aqueous phase. Environ Pollut 263, 114484. https://doi.org/10.1016/j.envpol.2020.114484.
[35] Liu, P., Zhan, X., Wu, X., Li, J., Wang, H., Gao, S., 2020. Effect of weathering on environmental behavior of microplastics: Properties, sorption and potential risks. Chemosphere 242, 125193. https://doi.org/10.1016/j.chemosphere.2019.125193.
[36] Liu, P., Wu, X., Peng, J., Wang, H., Shi, Y., Huang, H., Gao, S., 2021. Critical effect of iron red pigment on photoaging behavior of polypropylene microplastics in artificial seawater. J Hazard Mater 404, 124209. https://doi.org/10.1016/j.jhazmat.2020.124209.
[37] Lomakin, S., Mikheev, Y., Usachev, S., Rogovina, S., Zhorina, L., Perepelitsina, E., Levina, I., Kuznetsova, O., Shilkina, N., Iordanskii, A., Berlin, A., 2024. Evaluation and modeling of polylactide photodegradation under ultraviolet irradiation: Bio-based polyester photolysis mechanism. Polymers 16, 985. https://doi.org/10.3390/polym16070985.
[38] Luan, P., Oehrlein, G.S., 2019. Characterization of ultrathin polymer films using p-polarized ATR-FTIR and its comparison with XPS. Langmuir 35 (12), 4270–4277. https://doi.org/10.1021/acs.langmuir.9b00316.
[39] Luo, D., Luo, W., He, D., Wen, Q., Luo, S., Chen, K., Li, Y., Liu, C., Reinfelder, J.R., Huang, W., Chen, C., 2025. Polyethylene microplastics and nanoplastics colored with inorganic pigments in aquatic environments: Effects of mechanical aging on physicochemical properties, aggregation kinetics, and metal release. J Hazard Mater 496, 139233. https://doi.org/10.1016/j.jhazmat.2025.139233.
[40] Luo, H., Li, Y., Zhao, Y., Xiang, Y., He, D., Pan, X., 2020. Effects of accelerated aging on characteristics, leaching, and toxicity of commercial lead chromate pigmented microplastics. Environ Pollut 257, 113475. https://doi.org/10.1016/j.envpol.2019.113475.
[41] Luo, L., Zhang, T., Wang, M., Yun, R., Xiang, X., 2020. Recent advances in heterogeneous photo-driven oxidation of organic molecules by reactive oxygen species. ChemSusChem 13 (19), 5173–5184. https://doi.org/10.1002/cssc.202001398.
[42] Martí, E., Martin, C., Galli, M., Echevarría, F., Duarte, C.M., Cózar, A., 2020. The colors of the ocean plastics. Environ Sci Technol 54 (11), 6594–6601. https://doi.org/10.1021/acs.est.9b06400.
[43] Mo, X., Lu, X., Yang, S., Tan, Y., Fu, H., Zhu, D., Qu, X., 2025. Strong photochemical activity of colored microplastics containing cadmium pigments: Mechanisms and implications. Environ Sci Technol 59 (14), 7357–7365. https://doi.org/10.1021/acs.est.4c14715.
[44] Momma, K., Izumi, F., 2008. VESTA: A three-dimensional visualization system for electronic and structural analysis. J Appl Crystallogr 41, 653–658. https://doi.org/10.1107/S0021889808012016.
[45] Monclús, L., Lopez-Bejar, M., De la Puente, J., Covaci, A., Jaspers, V.L.B., 2019. Can variability in corticosterone levels be related to POPs and OPEs in feathers from nestling cinereous vultures (*Aegypius monachus*)? Sci Total Environ 650, 184–192. https://doi.org/10.1016/j.scitotenv.2018.08.188.
[46] Murphy, J., 2001. Additives for Plastics Handbook. Elsevier Science Inc, 360 Park Avenue South, New York, USA.
[47] Neese, F., 2012. The ORCA program system. WIREs Comput Mol Sci 2 (1), 73–78. https://doi.org/10.1002/wcms.81.
[48] Neubauer, N., Scifo, L., Navratilova, J., Gondikas, A., Mackevica, A., Borschneck, D., Chaurand, P., Vidal, V., Rose, J., Von der Kammer, F., Wohlleben, W., 2017. Nanoscale coloristic pigments: Upper limits on releases from pigmented plastic during environmental aging, in food contact, and by leaching. Environ Sci Technol 51 (20), 11669–11680. https://doi.org/10.1021/acs.est.7b02578.
[49] Okamoto, K., Nomura, M., Horie, Y., Okamura, H., 2022. Color preferences and gastrointestinal-tract retention times of microplastics by freshwater and marine fishes. Environ Pollut 304, 119253. https://doi.org/10.1016/j.envpol.2022.119253.
[50] OSHA Occupational Chemical Database. Occupational Safety and Health Administration. ⟨https://www.osha.gov/chemicaldata⟩. (Accessed on July 19th, 2025).
[51] Peeken, I., Primpke, S., Beyer, B., Gütermann, J., Katlein, C., Krumpen, T., Bergmann, M., Hehemann, L., Gerdts, G., 2018. Arctic sea ice is an important temporal sink and means of transport for microplastic. Nat Commun 9 (1), 1505. https://doi.org/10.1038/s41467-018-03825-5.
[52] Pritchard, G., 1998. Plastics Additives. Springer, Dordrecht, the Netherlands.
[53] Rojas-Poblete, M., Carreño, A., Gacitúa, M., Páez-Hernández, D., Rabanal-León, W. A., Arratia-Pérez, R., 2018. Electrochemical behaviors and relativistic DFT calculations to understand the terminal ligand influence on the $[Re_6(\mu_3\text{-}Q)_8X_6]^{4-}$ clusters. N J Chem 42, 5471–5478. https://doi.org/10.1039/C7NJ05114J.
[54] Stephens, P.J., Devlin, F.J., Chabalowski, C.F., Frisch, M.J., 1994. *Ab initio* calculation of vibrational absorption and circular dichroism spectra using density functional force fields. J Phys Chem 98 (45), 11623–11627. https://doi.org/10.1021/j100096a001.
[55] Su, J., Ruan, J., Luo, D., Wang, J., Huang, Z., Yang, X., Zhang, Y., Zeng, Q., Li, Y., Huang, W., Cui, L., Chen, C., 2023. Differential photoaging effects on colored nanoplastics in aquatic environments: Physicochemical properties and aggregation kinetics. Environ Sci Technol 57 (41), 15656–15666. https://doi.org/10.1021/acs.est.3c04808.
[56] Sun, Y., Zhang, J., Jiang, Z., Wang, Y., Duan, P., Min, W., Zhang, W., 2024. Polystyrene microplastics enhance oxidative dissolution but suppress the aquatic acute toxicity of a commercial cadmium yellow pigment under simulated irradiation. J Hazard Mater 463, 132881. https://doi.org/10.1016/j.jhazmat.2023.132881.
[57] Thacharodi, A., Meenatchi, R., Hassan, S., Hussain, N., Bhat, M.A., Arockiaraj, J., Ngo, H.H., Le, Q.H., Pugazhendhi, A., 2024. Microplastics in the environment: A critical overview on its fate, toxicity, implications, management, and bioremediation strategies. J Environ Manag 349, 119433. https://doi.org/10.1016/j.jenvman.2023.119433.
[58] Tian, L., Chen, Q., Jiang, W., Wang, L., Xie, H., Kalogerakis, N., Ma, Y., Ji, R., 2019. A carbon-14 radiotracer-based study on the phototransformation of polystyrene nanoplastics in water versus in air. Environ Scinano 6 (9), 2907–2917. https://doi.org/10.1039/C9EN00662A.
[59] Tigner, J.M., Elmer-Dixon, M.M., Maurer-Jones, M.A., 2023. Quantification of polymer surface degradation using fluorescence spectroscopy. Anal Chem 95, 9975–9982. https://doi.org/10.1021/acs.analchem.3c01151.
[60] Turner, A., 2019. Cadmium pigments in consumer products and their health risks. Sci Total Environ 657, 1409–1418. https://doi.org/10.1016/j.scitotenv.2018.12.096.
[61] Ugwu, K., Herrera, A., Gómez, M., 2021. Microplastics in marine biota: A review. Mar Pollut Bull 169, 112540. https://doi.org/10.1016/j.marpolbul.2021.112540.
[62] Vosko, S.H., Wilk, L., Nusair, M., 1980. Accurate spin-dependent electron liquid correlation energies for local spin density calculations: A critical analysis. Can J Phys 58 (8), 1200–1211. https://doi.org/10.1139/p80-159.
[63] Wang, H., Liu, P., Wang, M., Wu, X., Shi, Y., Huang, H., Gao, S., 2021. Enhanced phototransformation of atorvastatin by polystyrene microplastics: Critical role of aging. J Hazard Mater 408, 124756. https://doi.org/10.1016/j.jhazmat.2020.124756.
[64] Wen, B., Liu, J.-H., Zhang, Y., Zhang, H.-R., Gao, J.-Z., Chen, Z.-Z., 2020. Community structure and functional diversity of the plastisphere in aquaculture waters: Does plastic color matter? Sci Total Environ 740, 140082. https://doi.org/10.1016/j.scitotenv.2020.140082.
[65] Wei, P., Tang, M., Wang, Y., Wang, J., Wang, Y., Liu, H., Qiu, M., Qu, X., Yang, K., 2025. Toxic effect and the mechanisms of colored microplastics containing inorganic pigments on Microcystis aeruginosa. Ecotox Environ Safe 307, 119428. https://doi.org/10.1016/j.ecoenv.2025.119428.
[66] Xu, D., Wang, H., Zhang, K., Ya, Z., Wang, H., Zhang, S., 2025. Photocatalytic waste polystyrene plastic conversion: Reaction mechanism and catalyst design. Environ Sci Technol 59 (31), 16112–16129. https://doi.org/10.1021/acs.est.5c07160.
[67] Yousif, E., Haddad, R., 2013. Photodegradation and photostabilization of polymers, especially polystyrene: Review. SpringerPlus 2 (1), 398. https://doi.org/10.1186/2193-1801-2-398.
[68] Zhang, Z., Hirose, T., Nishio, S., Morioka, Y., Azuma, N., Ueno, A., Ohkita, H., Okada, M., 1995. Chemical recycling of waste polystyrene into styrene over solid

acids and bases. Ind Eng Chem Res 34 (12), 4514–4519. https://doi.org/10.1021/ie00039a044.

[69] Zhang, Y., Wu, P., Xu, R., Wang, X., Lei, L., Schartup, A.T., Peng, Y., Pang, Q., Wang, X., Mai, L., Wang, R., Liu, H., Wang, X., Luijendijk, A., Chassignet, E., Xu, X., Shen, H., Zheng, S., Zeng, E.Y., 2023. Plastic waste discharge to the global ocean constrained by seawater observations. Nat Commun 14 (1), 1372. https://doi.org/10.1038/s41467-023-37108-5.

[70] Zhao, X., Wang, J., Leung, K.M.Y., Wu, F., 2022. Color: An important but overlooked factor for plastic photoaging and microplastic formation. Environ Sci Technol 56 (13), 9161–9163. https://doi.org/10.1021/acs.est.2c02402.

[71] Zhong, S., Li, R., Tian, Y., Wei, Z., Zhang, L., Chen, Y., Zhou, R., Zhang, Q., Ru, X., 2024. Integrative models for environmental forecasting of phthalate migration from microplastics in aquaculture environments. J Hazard Mater 480, 136194. https://doi.org/10.1016/j.jhazmat.2024.136194.

[72] Zhu, K., Jia, H., Zhao, S., Xia, T., Guo, X., Wang, T., Zhu, L., 2019. Formation of environmentally persistent free radicals on microplastics under light irradiation. Environ Sci Technol 53 (14), 8177–8186. https://doi.org/10.1021/acs.est.9b01474.

[73] Zuo, L., Li, Y., Hou, W., Wang, F., Feng, Y., Zhang, Z., 2023. Leaching of triphenyl phosphate and tri-*n*-butyl phosphate from polystyrene microplastics: Influence of plastic properties and simulated digestive fluids. Environ Sci Pollut Res 30 (53), 114659–114666. https://doi.org/10.1007/s11356-023-30229-w.